Euler Homogeneity Equation in Source Parameter Imaging and Deconvolution for Depth-To-Basement Estimation of Ground Magnetic Survey Data

Samson Oyine Ankeli [1], **Musa Ayinde Tijani** [2], **Jeffrey Ilabeshi** [3]

[1] *Federal University of Technology Akure*
P. M. B. 704, Akure, Ondo State, Nigeria

[2] *King Saudi University*
Riyadh, Saudi Arabia

[3] *Federal Polytechnic Auchi*
Auchi, Edo State, Nigeria

DOI: 10.22178/pos.130-10

LCC Subject Category: T1-995

Received 26.04.2026
Accepted 25.05.2026
Published online 31.05.2026

Corresponding Author:
Samson Oyine Ankeli

Abstract. This study investigated the depth to bedrock of the Aule Flood landscape using Source Parameter Imaging (SPI) and the Euler deconvolution depth estimation algorithm, which applies Euler homogeneity equations to the acquired ground magnetic potential data. The study used the structural index (N) to describe the shape of the underlying causative body. Euler deconvolution employs the homogeneity equation to precisely measure the potential field and estimate the depth and location of the source causative body. The SPI-based depth estimation technique calculates the local wavenumber and the analytical signal using the Euler homogeneity equation. The observed vertical and horizontal derivatives of the Earth's magnetic field are combined to obtain the local wave number. Conforming to the preliminary findings of the ground magnetic exploration, Euler deconvolution estimated the deepest possible basement level at 31.9.

In comparison, Source Parameter Imaging (SPI) estimated a maximum depth of 74.9 meters. This study shows that the Euler Deconvolution method is more sensitive to shallow magnetic sources than to deeper ones because it uses the vertical derivative, which amplifies shallow-source anomalies. Because the SPI approach is not affected by magnetisation direction, it can provide precise depth estimates in the vicinity of this study. The studied geographic region's bedrock relief portrays an uneven geologic succession with several bedrock deformations, as indicated by results from Source parameter imaging and the Euler deconvolution method for depth estimation, due to broken bedrock and buried metal resources underlying various locations. Since the results obtained support the geology of the research area, these depth-estimating methods are highly reliable.

Keywords: Bedrock relief; Homogeneity Equation; Depth estimation; geophysics.

INTRODUCTION

Determining the depth to bedrock using geophysical methods is crucial to reducing the risk of collapse of national infrastructure, including roads, bridges, buildings, and dams. Researchers worldwide have made numerous contributions to the depth estimation of potential field data and have widely used the Euler equations to estimate the depth of subsurface sources in prospective geophysical investigation areas. The Euler depth estimator is one of the most popular techniques among the many developed to rapidly identify the geometrical properties of sought-after sources that may be causing field abnormalities.

One of this algorithm's main advantages is its speed and simplicity, which provide a foundation for further in-depth research, modelling, and interpretation [1]. The Euler deconvolution and Source Parameter Imaging algorithm has several significant uses, including determining the depth of mineral deposits, locating possible field anomalies and shallow faults, determining the depth of geothermal reservoirs, and determining the thickness of surface sediments [2–4]. The limits of anomalies and the depth of discontinuities, for example, can be determined using the Euler set of equations, in addition to depth estimation [5, 6]. The Euler equations are used to accurately determine the depth of subsurface sources from potential-field horizontal and vertical derivatives. To the best of our knowledge, the author [7] was the first to propose and refine this strategy based on a profile of possible field data. Authors [5] then solved the equations for 2D data.

In Nigeria, construction collapses are disconcerting and terrifying for nearby communities. One of the ways that people lose their lives and property is through building collapses. According to earlier research, magnetic susceptibility measurements have revealed bedrock, magnetic minerals, contact between different rock types, fractures, lineaments, faults, and rock boundaries [8]. Accurately measuring anomalies has become considerably easier with the adoption of magnetic techniques in geophysical research. Variations in the degree of magnetisation continuously forming in rocks cause anomalies in the local Earth magnetic field. Rock magnetisation is induced by either remanent magnetisation or the Earth's magnetic field. The amount of remanence that remains after a lengthy period of time is the final factor that determines the intensity of induction, along with the rock's magnetic susceptibility and magnetising force [9]. This study used the ground magnetic method to determine the location of rock structures and the depth to bedrock relief at the Aule flood zone Fadama rice field in Akure South, Ondo State. This method has an advantage across a wide land mass because it is quick and efficient. To prevent sinking, differential settlement, and cracks in the structures to be built in the research area, this investigation is necessary. Road failures, building cracks, and structural collapses were caused by a lack of understanding of the subsurface [10].

Euler Deconvolution method. The Euler homogeneity equation expresses magnetic or gravitational potential field data. This formula precisely calculates the potential field and the depth and location of the causative body. The term structural index (N) describes the form of the causative source body. Euler Deconvolution is the name of this technique [11].

If U is a function of three variables f(x, y, z) of a degree n that satisfies the condition for any scalar for t > 0 $x = xt, y = yt, z = zt$

$$U = f(tx, ty, tz) \tag{1}$$

$$U = t^n f(x, y, z) \text{ this implies} \tag{2}$$

$$f(tx, ty, tz) = t^n f(x, y, z) \tag{3}$$

Considering a potential magnetic field P whose attributes are functions of coordinates (x, y, z) and of the point source $(x_o\, y_o\, z_o)$ coordinates. If we test for homogeneity at a distance from the point source, i.e $(x - x_o), (y - y_o), (z - z_o)$. Let r represent the relative coordinates from the point source:

$$rx = (x - x_o), ry = (y - y_o), rz = (z - z_o),$$

If we define the magnetic field P(x, y, z) relative to the point source (x_o, y_o, z_o), which is a function of the distance vector

$$r = rxi + ryj + rzk \tag{4}$$

$$r = (x - x_o)i + (y - y_o)j + (z - z_o)k \tag{5}$$

Recall equation 3

$$f(tx, ty, tz) = t^n f(x, y, z)$$

The function P satisfy the scalar factor t > 0 to achieve homogeneity.

$$P[t(x - x_o), t(y - y_o), t(z - z_o)] =$$
$$= t^n P(x - x_o, y - y_o, z - z_o) \tag{6}$$

Differentiating with respect to t

$$\frac{\partial}{\partial t}[\mathrm{P(t(x - x_o), t(y - y_o), t(z - z_o)}] =$$

$$= \frac{\partial}{\partial t}[\text{tn P}(\text{x-x}_o, \text{y-y}_o, \text{z-z}_o)]$$

to the first part of the equation

$$\frac{\partial}{\partial t}[P(t(x-x_o), t(y-y_o), t(z-z_o)] =$$
$$= \frac{\partial P}{\partial x} \times \frac{dx}{dt} + \frac{\partial P}{\partial y} \times \frac{dy}{dt} + \frac{\partial P}{\partial z} \times \frac{dz}{dt}$$

Since

$$x = t(x-x_o) \ \frac{dx}{dt} = (x-x_o), \ y = t(y-y_o),$$
$$\frac{dy}{dt} = (y-y_o) \ z = t(z-z_o)$$
$$\frac{dz}{dt} = (z-z_o) = \frac{\partial P}{\partial x}(x-x_o) + \frac{\partial P}{\partial y}(y-y_o) +$$
$$+ \frac{\partial P}{\partial z}(z-z_o)$$

To the second part of the equation

$$\frac{\partial}{\partial x}[\text{tn P}(x-x_o, y-y_o, z-z_o)]$$

since P does not depend on t

$$= t^n \times 0 + P \times nt^{n-1} = nt^{n-1}\text{P}$$
$$(x-x_o)\frac{\partial P}{\partial x} + (y-y_o)\frac{\partial P}{\partial y} + (z-z_o)\frac{\partial P}{\partial z} =$$
$$= nt^{n-1}P \quad (7)$$

when t = 1, it yields the Euler homogeneity equation in its standard form used in geophysics.

This gives

$$(x-x_o)\frac{\partial P}{\partial x} + (y-y_o)\frac{\partial P}{\partial y} +$$
$$+(z-z_o)\frac{\partial P}{\partial z} = nP \quad (8)$$

for the structural index N is defined by N = -n, applying the regional background field B to the equation

$$(x-x_o)\frac{\partial P}{\partial x} + (y-y_o)\frac{\partial P}{\partial y} + (z-z_o)\frac{\partial P}{\partial z} =$$
$$= N(P-B) \quad (10)$$

Author [7] showed that Euler's homogeneity relation could be expressed as equation (10).

Where $(x_o \, y_o \, z_o)$ is the location of the magnetic causative body, (x, y, z) are the measured points of the coordinate, P and B are the regional field whose total field magnetic anomaly at x, y, z, $\frac{\partial P}{\partial x}, \frac{\partial P}{\partial y}, \frac{\partial P}{\partial z}$ is the magnetic potential field's partial derivative with respect to x, y, z components. The solution to the equation is obtained by calculating the anomaly gradient for the various anomaly areas with structural index N, which is used to express the geometry of the source body; N = 0 for fault/contact, N = 1 for dyke, and N = 2 for pipes.

Source Parameter Imaging (SPI). The SPI method computes depth to magnetic source bodies by analysing the measured magnetic anomalies. Depth estimation using the SPI method requires computing the local wavenumber and the analytical signal. The local wavenumber is the sum of the vertical and horizontal derivatives of the measured Earth magnetic field. The Hilbert transform is applied to the original magnetic field data to estimate the analytical signal. The Analytical signal/total gradient is independent of the magnetisation source direction and the magnetisation field [12].

Recall equation (10)

$$(x-x_o)\frac{\partial P}{\partial x} + (y-y_o)\frac{\partial P}{\partial y} + (z-z_o)\frac{\partial P}{\partial z} =$$
$$= -N(P-B)$$

The Hilbert transform relates the derivative of the vertical magnetic field component to the derivative of the horizontal magnetic field component in a 2D case where the potential field $P(x, z)$ is measured along the x-axis and caused by a two-dimensional source aligned parallel to the y-axis, independent of x_o, y_o, z_o, and B:

$$\frac{\partial P}{\partial z} = -\mathcal{H}\frac{\partial P}{\partial x}$$

where $\mathcal{H}$ is the Hilbert transform, N = -n.

$$(x-x_o)\frac{\partial P}{\partial x} + (y-y_o)\frac{\partial P}{\partial y} + (z-z_o)\frac{\partial P}{\partial z} = nP$$
$$x\frac{\partial P}{\partial x} + z\frac{\partial P}{\partial z} = nP$$

(N = -n and x is independent of $x_o \, y_o \, z_o \, B$)

Analytical signal $A(x, z) = \frac{\partial P}{\partial x}i + \frac{\partial P}{\partial z}j$.

Authors [12, p. 352], Analytical amplitude along the x-axis is given by

$$|A(x)| = \sqrt{\left(\frac{\partial P}{\partial x}\right)^2 + \left(\frac{\partial P}{\partial z}\right)^2} \text{ where } i^2, j^2 = 1$$

For the 3D case, the Analytical signal A of a potential field $P(x, y, z)$ is given by the complex orthogonal derivative function [13, 14].

$$A(x, y, z) = \frac{\partial P}{\partial x} i + \frac{\partial P}{\partial y} j + \frac{\partial P}{\partial z} k$$

$$AS\ amplitude = \sqrt{\left(\frac{\partial P}{\partial x}\right)^2 + \left(\frac{\partial P}{\partial y}\right)^2 + \left(\frac{\partial P}{\partial z}\right)^2}$$

The spatial domain, which is a function of the Fourier transform of wavenumber k, which measures cycles per unit distance, is necessary for depth estimates of magnetic sources. Author [13] demonstrated the relationship between the imaginary and real components of the vertical and horizontal derivatives of a two-dimensional analytical signal.

$$\mathrm{A1}(x, y) = \frac{\partial P(x,z)}{\partial x} - j\frac{\partial P(x,z)}{\partial z}$$

$$\frac{\partial P(x, z)}{\partial x} = -\mathcal{H}\frac{\partial P(x, z)}{\partial z}$$

The local wave number correlates with the depth of magnetic source bodies; a greater wave number indicates shallower sources. Author [15] defines the local wave number as

$$K_1 = \frac{\partial}{\partial x}\tan^{-1}\left(\frac{\frac{\partial P}{\partial z}}{\frac{\partial P}{\partial x}}\right)$$

The analytical signal is obtained from the second-order derivative of the total field P; the vertical derivative is associated with the pair of Hilbert transforms.

$$\frac{\partial^2 P(x, z)}{\partial x^2} = -\mathcal{H}\frac{\partial^2 P(x, z)}{\partial z^2}$$

The analytical signal is defined by the second-order derivatives A2(x, z)

$$A_2(\mathrm{x, z}) = \frac{\partial^2 P(x, z)}{\partial x^2} - \mathrm{j}\frac{\partial^2 P(x, z)}{\partial z^2}$$

This gives rise to the second-order wavenumber K_2

$$\mathrm{K}_2 = \frac{\partial}{\partial x}\tan^{-1}\left(\frac{\frac{\partial^2 P}{\partial z^2}}{\frac{\partial^2 P}{\partial x^2}}\right)$$

Depth estimation $Z = 1/k$

Research site and Geology. The Aule area is designated primarily by the crystalline rock of the historic basement complex in southwest Nigeria [16]. The geological divisions are migmatite gneiss, charnokite gneiss, and granite [17]. The region's fluid geological environment enables the occurrence of many igneous and metamorphic rock types, but these rocks are often rigid outside cleaved, sheared, fractured, and fissured areas. The western portion of the research area hosts numerous biotite granitic gneiss formations and charnokite boulders. The twenty-two-acre rice field used for the third edition of the National Fadama Regional Growth Project Optional Financing resides near Motorway D4 Aule G.R.A. in the Akure South jurisdiction area of Ondo State (Figure 1).

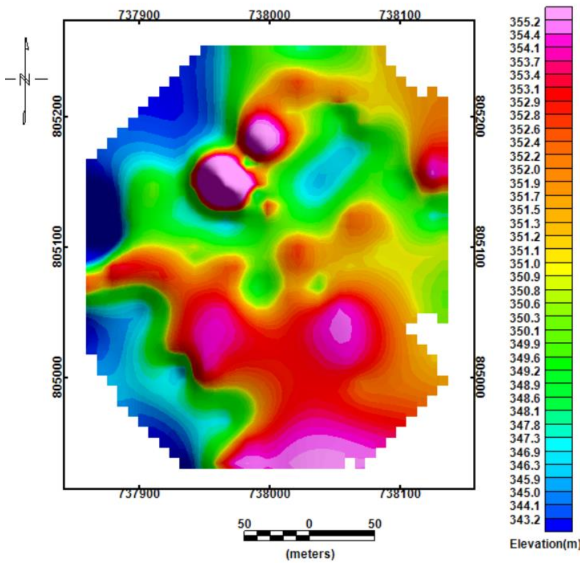

Figure 1 – Elevation of the Research Site

It is located between north coordinates 805227 Nm and 804983 Nm and east coordinates 737997 Em and 7379536 Em using the Unified Parallel Coordinates (UTM). An inundation overwhelmed the region. The illustration below depicts the general surface elevation of the research site.

METHODS

The entire strength of Earth's magnetic field, often called the total field, was measured using a proton precision magnetometer. This study used the pause-and-continue technique to collect the data. The technique is crucial for delineating subsurface depths greater than 20 m. During data acquisition, the study used a 20 m station spacing. The study measured and recorded the total field component at every station interval across the Fadama flood zone. It conducted a ground magnetic survey using a highly accurate, user-friendly proton-precession magnetometer. It collected the coordinates of each station using a GPS device. Three magnetic profiles were aligned for each of the three investigations, and the outcomes appeared as magnetic profiles with varying intensities. The profiles are 200 m long, with a station spacing of 20 m, and they are all oriented northwest to southeast. The study built a base station to precisely measure temporal variations in Earth's magnetic field and create accurate magnetic maps. The measured magnetic values for the three profiles were plotted against ground distance after the drift correction was applied. At each station point, this profile displays regions of high and low magnetic response.

Data Processing. The study first corrected the original magnetic data for drift and daily fluctuations to ensure accuracy. The study obtained the IGRF values for the stations, subtracted them from the data, and eliminated the core field component. Secular and diurnal fluctuations have therefore been taken into account. However, the resulting magnetic intensity map would still contain numerous components induced by crustal structures of varying sizes. Magnetic anomalies with extended spatial wavelengths, also known as regional anomalies, are produced by deep, large-scale structures. Conversely, shallower structures cause anomalies with shorter spatial wavelengths called residual anomalies. For the Regional-Residual distinction, an upward continuation of 100 m was utilised as a filtering technique, effectively reducing anomalies and suppressing high-wave-number or short-wavelength anomalies. Since the reduction-to-pole transformation accounts for asymmetry in magnetic field anomalies, which results in the peaks and troughs of the total field anomaly not being precisely above the causative body, it was used to replicate the anomaly as if it were at the pole. This transformation helps in accurately identifying the causative body [18].

Other components were then derived from the vertical component of the geomagnetic field. The analysis derived other components from the vertical component of the geomagnetic field. It then reduced the corrected data to the pole (RTP) to align the detected anomalies with their sources and reduce the effects of magnetic inclination and declination. This transformation used local geomagnetic parameters of $-10.6°$ inclination and $-3.0°$ declination. The workflow further processed the data using several derivative techniques, including Analytical Signal Amplitude (ASA), which identifies magnetic bodies by combining horizontal and vertical gradients.

Researchers used two main techniques for depth estimation: Standard Euler Deconvolution and Source Parameter Imaging (SPI). To decipher the subsurface structure, SPI provided direct depth estimates of magnetic sources. The Euler Deconvolution approach provided additional information about the distribution of subsurface features by estimating the depth and location of magnetic sources from magnetic field gradients. When combined, these techniques and maps, produced from processed ground magnetic data, provided a thorough understanding of the geological features in the research region, including information on faults, contacts, and other areas of interest for further investigation [18].

RESULTS AND DISCUSSION

Interpretation of Magnetic Maps. The map (Figure 2) revealed strong magnetic responses in the north, northwest, and south, which may be caused by buried metallic items or shallow bedrock.

The eastern and northeastern flanks of the research area exhibit a blue-hued zone with minimal magnetic response. Within the research area, intermediate green magnetic traces are visible in the western, central region that runs southeast. Differences in lithology, sedimentary thickness, and observed magnetic susceptibility may account for the highs and lows in the magnetic signals, explaining the distinction in basement topography.

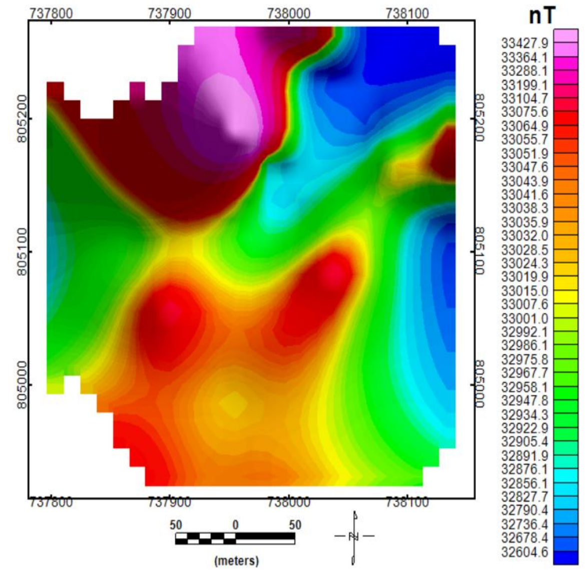

Figure 2 – Total Magnetic Intensity Map

Residual Map. After the IGRF correction has been executed, the regional magnetic field is eliminated from the Total Field, resulting in the residual map shown (in Figure 3), identical to the Total Field map.

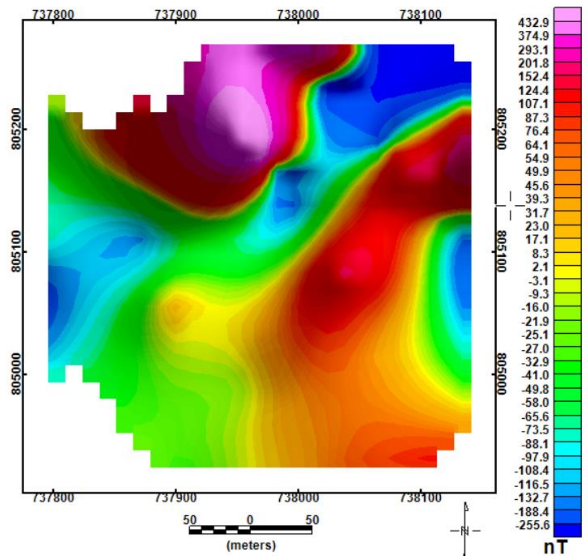

Figure 3 – Residual field map of the area

The derived Residual map shows highs in the northern and northeast-southern regions and lows in the eastern and northeastern margins of the research area. The observed magnetic strengths ranged from low -255.6 nT (blue) to high +432.9nT (pink). A green line extends from the northeast to the south and west of the area.

Analytical Signal Map. The research area's analytical signal showed amplitude variation ranging from -6.3 to +19.0, with the northern, northeastern, eastern, and western flanks exhibiting the highest amplitudes, as indicated by pink to red colours.

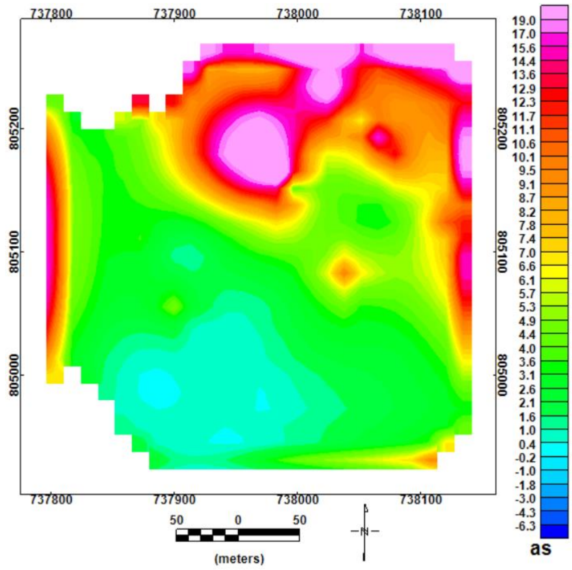

Figure 4 – Analytical Signal Map

A substantial signal amplitude variation of 1.0 to +9.1 was observed in the green-to-orange colour range. This amplitude signal extends across the northwest, south, and southeast portions of the research region, covering two-thirds of the region.

Euler Deconvolution. The Euler deconvolution method is noise-sensitive since it employs the magnetic map's first vertical derivative filter. The analysis applied a 50 m upward continuation filter to low signal-to-noise ratio data before performing Euler deconvolution. Estimates of depth may become uncertain due to the complex geometry of magnetic sources. The analysis calculated the Euler depths using the derivatives dx, dy, and dz. For shallow magnetic bodies, vertical derivatives are advantageous. shows the depths of buried potential-field bodies, which could be near-surface intrusive rocks or deep-seated basement rocks. Euler deconvolution of the magnetic field's analytic signal allows determination of the structural index and source parameters, provided the magnetic field is contaminated only by a constant ground intensity [19]. As a result, the analysis selected a structural index of one (N = 1), and the results matched those obtained by deconvolving the magnetic field under the influence of a steady baseline field [19].

Source Parameter Imaging (SPI) Result. Three derivative grids in the x-, y-, and z-directions are required to compute source-parameter imaging. To perform this depth-estimation method, the dx, dy, and dz components of the magnetic residual data were processed using Oasis Montaj version 8.4. The resultant grids, dx, dy, and dz, were then used as input grids in the SPI processing tool on the Oasis Montaj software menu bar. The Tilt derivative grid, SPI values, and other peak values were obtained by calculating the Source Parameter Imaging. The analysis also applied a first-order derivative filter to the estimated values. This step guarantees an accurate determination of the local wave count.

The study then computed the depth to magnetic sources from the acquired digitised ground magnetic data to evaluate source depth quantitatively [20]. The Source parameter imaging grid shown on a map is created by gridding the estimated Source parameter imaging values.

Comparison of the Source Parameter Imaging (SPI) and Euler deconvolution Methods. The Source Parameter Imaging Figures 5 show the depth to source bodies with magnetic signatures occurring within the subsurface of the study area.

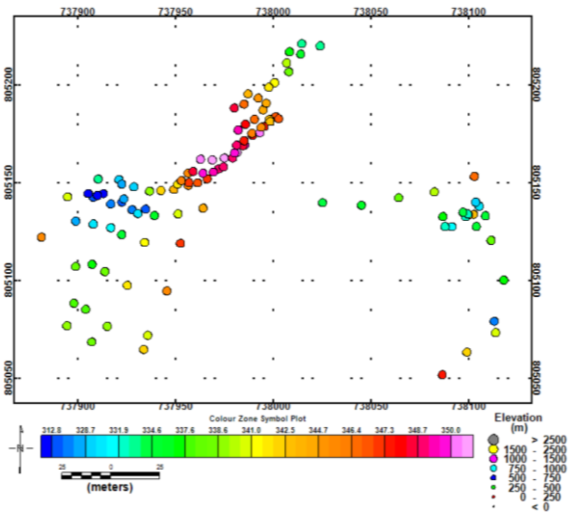

Figure 5a – 3D Euler depth solution map shows the cluster of source depth locations positioned at the boundaries

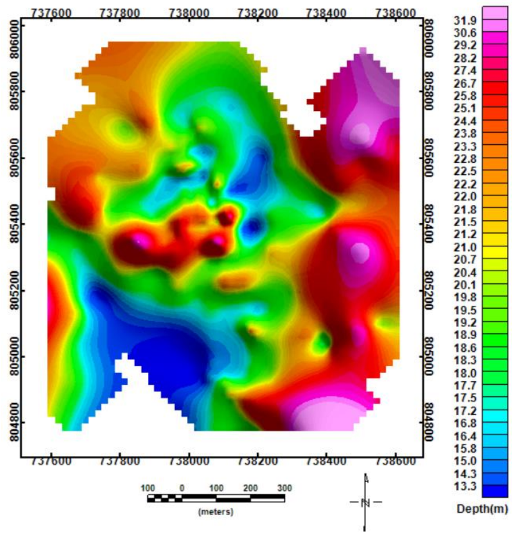

Figure 5b – 3D Euler depth estimates at N = 0

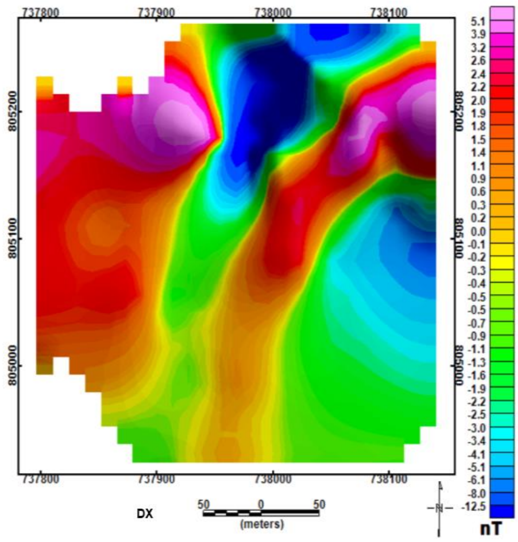

Figure 5c (DX) – X-directional Derivative

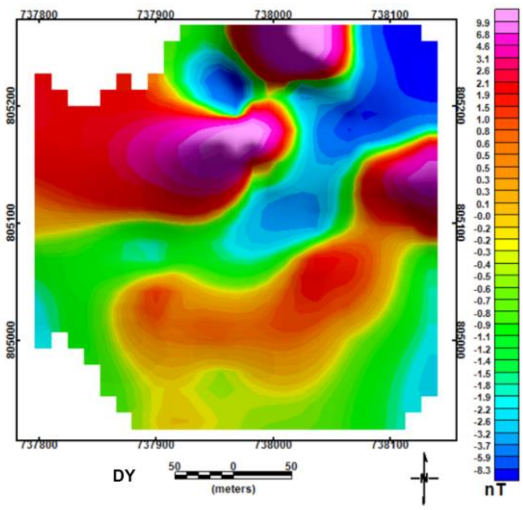

Figure 5d (DY) – Derivative in the Y-direction

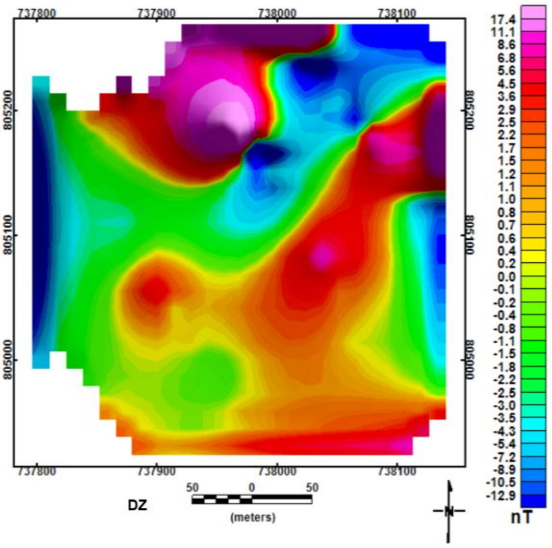

Figure 5e (DZ) – Derivative in the Z-direction

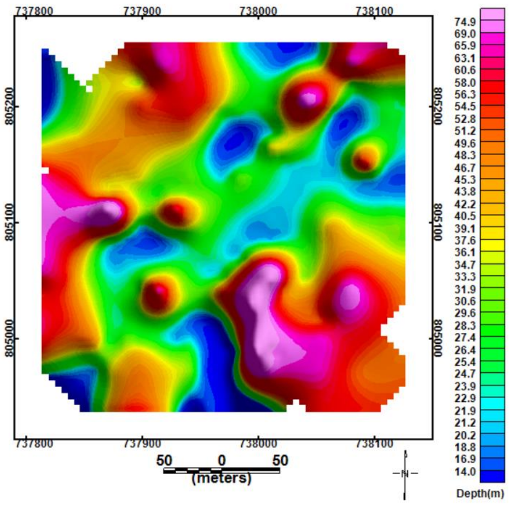

Figure 5 – Source Parameter Imaging Result

We can therefore categorise the SPI map into deep-seated sources, medium-seated bodies, and shallow-seated bodies occurring in the subsurface of the study area. This depth variation is distributed across the study area, ranging from 74.9 m to 14.0 m. Deep-seated bodies and medium-seated sources predominate within the study area. The deep basement is represented in pink to red, the medium-depth response from magnetic sources in green to orange, and shallow-depth classification in blue, representing response from shallow-seated bodies.

Following Euler deconvolution, the Standard Euler depth map shows a depth variation of 13.3 to 31.9 m. Areas with deep-seated bodies are typically indicated by the colours pink and red, whereas the colour blue indicates areas with shallow-lying magnetic potential field bodies. Deep-seated bodies dominate the eastern, northeast-southeast, and central regions of the research area. The depth of intermediate magnetic bodies, which run from north to south of the field, is shown by the green-yellow colour. The blue colour indicates shallowly seated magnetic bodies, primarily located in the southwestern portion of the research area; this may occur because the Euler Deconvolution method uses the vertical derivative, which amplifies shallow sources and makes it more sensitive to their depths than to those of deeper sources.

In the study region, which is the stable portion of the platform, the SPI depth estimates are typically appropriate. Furthermore, areas with significant depth variations are typically deep or have low magnetic susceptibility. Because of the high likelihood of remanent magnetisation, only the SPI method, which is unaffected by magnetisation direction, can provide precise depth estimates for this study region.

CONCLUSIONS

Euler deconvolution of the magnetic field's analytic signal permits the computation of the structure index and source parameter images, provided the magnetic field is contaminated only by an unchanging origin threshold. The research area's bedrock relief exhibits an uneven geologic succession with several bedrock depressions. According to results from Source parameter imaging and the Euler deconvolution method for depth estimation, broken bedrock and buried metal resources underlie some areas. The results obtained support the geology of the research area; these depth-estimating methods are highly reliable.

REFERENCES

1. Ghanbarifar, S., Hosseini, S. H., Ghiasi, S. M., Abedi, M., & Afshar, A. (2024). Joint Euler deconvolution for depth estimation of potential field magnetic and gravity data. *DOAJ (DOAJ: Directory of Open Access Journals)*. doi: 10.22059/ijmge.2023.363558.595090

2. Hosseini, S. H., Dehkordi, B. H., Abedi, M., & Oskooi, B. (2020). Implications for a geothermal reservoir at Abgarm, Mahallat, Iran: Magnetic and magnetotelluric signatures. *Natural Resources Research, 30*(1), 259–272. doi: 10.1007/s11053-020-09739-8

3. Ghiasi, S. M., Hosseini, S. H., Afshar, A., & Abedi, M. (2022). A novel magnetic interpretational perspective on Charmaleh iron deposit through improved edge detection techniques and 3D inversion approaches. *Natural Resources Research, 32*(1), 147–170. doi: 10.1007/s11053-022-10135-7

4. Okpoli, C. C. (2019). High-Resolution Magnetic Field Signatures Over Akure and Its Environs, Southwestern Nigeria. *Earth Science Malaysia*, 09–17. doi: 10.26480/esmy.01.2019.09.17

5. Reid, A. B., Ebbing, J., & Webb, S. J. (2014). Avoidable Euler Errors – the use and abuse of Euler deconvolution applied to potential fields. *Geophysical Prospecting, 62*(5), 1162–1168. doi: 10.1111/1365-2478.12119

6. Reid, A. B., & Thurston, J. B. (2014). The structural index in gravity and magnetic interpretation: Errors, uses, and abuses. *Geophysics, 79*(4), 61–66. doi: 10.1190/geo2013-0235.1

7. Thompson, D. T. (1982). EULDPH: A new technique for making computer-assisted depth estimates from magnetic data. *Geophysics, 47*(1), 31–37. doi: 10.1190/1.1441278

8. Alagbe, O. A. (2013). Fracture Distribution within Bowen University Permanent Site and Its Hydrogeologic Implication. *Research Journal of Physical Sciences, 1*(3), 1-5.

9. Parasnis, D. S. (1986). *Principles of Applied Geophysics*. Chapman and Hall.

10. Adagunodo, T. A., Sunmonu, L. A., & Adabanija, M. A. (2015). Geomagnetic Signature Pattern Of Industrial Layout Orile Igbon. *Advances in Architecture, City and Environment, 1*(3), 14-25

11. Reid, A. B., Allsop, J. M., Granser, H., Millett, A. J., & Somerton, I. W. (1990). Magnetic interpretation in three dimensions using Euler deconvolution. *Geophysics, 55*(1), 80–91. doi: 10.1190/1.1442774

12. Blakely, R. J. (1996). *Potential Theory in Gravity and Magnetic Applications.* Cambridge University Press.

13. Nabighian, M. N. (1972). The analytic signal of two-dimensional magnetic bodies with polygonal cross-section; its properties and use for automated anomaly interpretation. *Geophysics, 37*(3), 507–517. doi: 10.1190/1.1440276

14. Nabighian, M. N. (1974). Additional comments on the analytic signal of two-dimensional magnetic bodies with polygonal cross-section. *Geophysics, 39*(1), 85–92. doi: 10.1190/1.1440416

15. Smith, R. S., Thurston, J. B., Dai, T., & MacLeod, I. N. (1998). iSPITM— the improved source parameter imaging method. *Geophysical Prospecting, 46*(2), 141–151. doi: 10.1046/j.1365-2478.1998.00084.x

16. Adelusi, A., Akinlalu, A. A., & Adebayo, S. S. (2013). Geophysical and hydrochemistry methods for mapping groundwater contamination around Aule area, Akure, Southwestern Nigeria. *International Journal of Water Resources and Environmental Engineering, 5*(7), 442–451. doi: 10.5897/ijwree2013.0370

17. Ankeli, S. O., Chukwuma, E. O., Kareem, T., & Adebisi, S. T. (2025). Subsurface Characterisation Using the Electrical Resistivity Method: A Case Study of Itohan Girls Grammar School, Benin City, Nigeria. *Path of Science, 11*(11), 9001. doi: 10.22178/pos.124-38

18. Ankeli, S. O., Kareem, T., Abioye, I. K., Ahamefule, F. C., Ahamefule, P. C., & Atoyebi, E. O. (2026). Integrated Geophysical Techniques for Near-Surface Engineering Studies at Fadama Rice Farm, Aule, Nigeria. *Path of Science, 12*(1), 7001. doi: 10.22178/pos.126-16

19. Keating, P., & Pilkington, M. (2004). Euler deconvolution of the analytic signal and its application to magnetic interpretation. *Geophysical Prospecting, 52*(3), 165–182. doi: 10.1111/j.1365-2478.2004.00408.x

20. Ayuba, R. A., & Nur, A. (2018). Depth Estimates Deduced From Source Parameter Imaging of High Resolution Aeromagnetic Data over Part of Nasarawa and Environs, North-Central Nigeria. *International Journal of New Technology and Research, 4*(4), 54-62.